

Atmospheric Characterization of Super-Earth 55 Cancri e

Departmental Honors Thesis

Michael Bess

Advisor: Diana Dragomir

Table of Contents

Abstract.....2
Background.....2
Research Question.....3
Method.....5
Data Analysis.....10
Results and Discussion.....15
Conclusion and Future Work.....16
Acknowledgements.....16
References.....17
Other Packages.....18

Abstract

55 Cancri e is the first small, rocky exoplanet lacking a hydrogen dominated atmosphere where an atmosphere has been confirmed [3]. Previous observations with Spitzer show heat redistribution on this planet [2] and two scenarios were created to explain this – a thick atmosphere, or a thin mineral atmosphere with asynchronous rotation. These observations also ruled out H₂O, CO₂, and CO as being the dominant component of the atmosphere [2]. Four atmospheric models were created by Angelo & Hu [5] as the most likely scenarios for 55 Cancri e’s atmosphere- N₂, N₂ with inversion, O₂, and SiO. Using the James Webb Space Telescope’s (JWST’s) NIRCam instrument a secondary eclipse of the planet was observed in the 3.8-to-5.1-micron wavelength in the near-infrared to obtain a precise measurement of the thermal emission of 55 Cancri e. This range tests for spectral features of CO and CO₂ which are most apparent in the N₂ models. Through analysis of this data, we determine that the N₂ and O₂ models can be ruled out, and the SiO and N₂ with inversion models appear to be the most promising. Further observation with JWST’s MIRI instrument in the 5-to-12-micron range has been done and analysis is ongoing to distinguish between these two scenarios, as a large SiO feature is prominent in this range.

Background

Exoplanets, or planets that orbit stars other than our own, are a crucial area of study in space exploration and discovery. They provide us with valuable information about the formation and evolution of planetary systems, and how they are populated throughout the universe. One key aspect of exoplanet research is determining the composition of their atmosphere’s, which can tell us a great deal about how the planet formed and how the system has evolved through its history. Atmospheres are also main indicators in determining if the planet could be suitable for life.

55 Cancri e is a super-Earth planet located 41 light years away. Super-Earth planets are a unique group of planets that we do not see in our solar system. They are rocky like our inner planets, but much larger. This planet is about 8 times more massive than the Earth and has a radius that is almost double that of Earth with a similar density. This planet orbits a K-type star in a binary star system, and it is the closest of the 4 confirmed planets in that system. K-type stars are slightly smaller, less massive, and less bright than our sun.

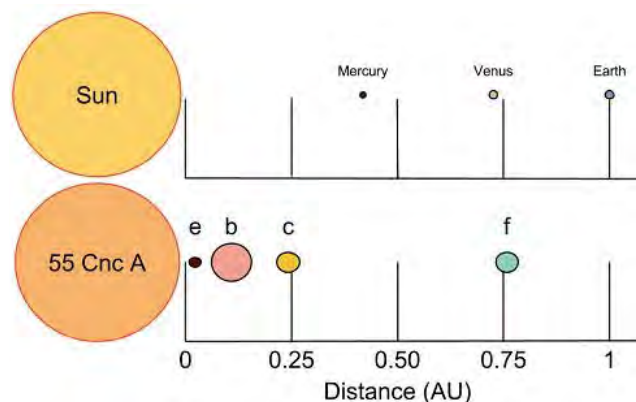


Figure 1: Comparison of the 55 Cancri A system to our Solar System [4].

This planet has an orbital period of about 0.74 days [1] or close to 18 hours, which means it is extremely close to its star, much closer than any planet in our own solar system. A comparison of this is displayed in Figure 1. It has a distance from its star of only 0.0152 astronomical units (AU) [1] compared to Mercury's semi major axis of about 0.4 AU. This means that 55 Cancri e is 26 times closer to its star than Mercury is to the sun and 65 times closer than Earth. As a result of it being so close to its star, the planet is very hot with dayside temperatures of about 2700 Kelvin and nightside temperatures of approximately 1400 Kelvin [2].

This planet presents a unique opportunity to characterize a sparsely explored region of exoplanets. Small exoplanets provide insight into planet formation and evolution that is not seen in our Solar System. One key question to answer for these types of exoplanets is whether or not they have an atmosphere, and if so, what the atmosphere is made of. Larger planets are expected to have atmospheres mainly comprised of hydrogen and helium that are retained from their formation, while smaller planets are not expected to have such atmospheres and could have no atmosphere at all as they are not able to retain their primordial atmospheres [3].

The James Webb Space Telescope (JWST) is a revolutionary instrument that is set to transform our understanding of our universe, and in particular, exoplanets. This incredible telescope boasts an unprecedented level of sensitivity and precision, allowing scientist to study exoplanets in a way that was never possible. The JWST is equipped with a suite of instruments that enable it to observe in a range of wavelengths from the near-infrared to the mid-infrared. Its capabilities include the ability to detect the chemical composition of exoplanet atmospheres and identify atmospheric features. With its unparalleled sensitivity, JWST will allow us to study exoplanets in greater detail than ever before, which is why this telescope was chosen to perform this observation.

Research Question

In previous observations of 55 Cancri e, the planet's thermal phase curve, observed by Spitzer in 2016, showed a peak in thermal emission prior to the eclipse indicating heat redistribution [2]. We would expect to see the peak of thermal emission right before the start of the eclipse if there is no heat redistribution on the planet. The fact that the peak is slightly shifted to before the start of eclipse, shows that the hottest part of the planet is not the side of the star that is directly facing the star, instead it includes part of the nightside of the planet. Analysis of that data showed that it would not be explained by heat transport due to currents in a molten lava ocean [6]. There are two main mechanisms for heat redistribution that could explain this phenomenon - having a thick atmosphere or having an asynchronous rotation.

For thick atmospheres, heat is redistributed through winds, causing heat from the dayside of the planet to warm the dark night side. An asynchronous rotation naturally redistributes heat as the planet rotates and different parts of the planet are warmed during its orbit. Small planets close

to their stars are generally believed to be tidally locked [5], meaning that the same side of the planet is always facing the star, and thus have large temperature swings from their dayside to their nightside. To produce heat redistribution in this scenario would require a thick atmosphere to warm the night side of the planet that receives to star light.

On the other hand, if this planet has an asynchronous rotation, it would create a natural means of heat redistribution without the need of a thick atmosphere. The goal of the observation of 55 Cancri e is to determine whether the heat redistribution on the planet is driven by the asynchronous rotation or thick atmosphere scenario.

In the asynchronous rotation scenario, we would expect to detect a thin mineral atmosphere formed from evaporation of rock on the dayside of the planet and subsequent condensation as the planet cools [7]. This would present a planet lacking a thick atmosphere with a molten lava surface which is shrouded by a thin mineral atmosphere dominated by Na, O, K, Fe, and SiO. SiO would be easy to detect in this atmosphere with large emission bands in the mid-infrared wavelengths [8].

Alternatively, if the planet has a thick atmosphere, we would assume the planet is tidally locked as a result of its short orbital period. This scenario requires the presence of a volatile rich atmosphere larger than approximately 1.4 bar [3]. Previous observations with the Spitzer telescope have ruled out the possibility of an atmosphere dominated by H₂O, CO₂, or CO due to the lack of strong absorption in the 4.5-micron channel observed [2]. The primary component of the atmosphere would thus be either N₂ or O₂ [9]. The presence of an O₂-dominated atmosphere is believed to have formed from the loss of hydrogen from a world once covered in a large water ocean. An N₂-dominated atmosphere would have formed by the accretion of rocky planetesimals and could have varying abundances of CO₂, CO, and HCN [3].

To distinguish between the two scenarios, a secondary eclipse of 55 Cancri e was observed to provide a thermal emission spectrum in the mid-infrared wavelength. An observation has been done using JWST's NIRCам instrument to provide emission spectrums in the 3.8 to 5.1-micron range (NIRCам F444W) to search for different spectral features pertaining to our two scenarios.

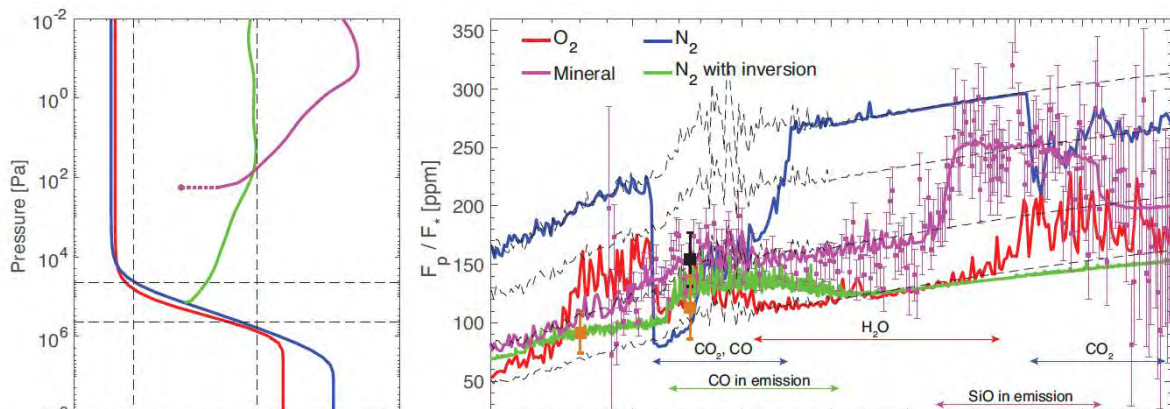


Figure 2: Left: Pressure-temperature profiles of the four models [3]. Right: Simulated emission spectra of the four atmospheric models [3].

Both scenarios have distinct features in the mid-infrared which makes it a prime candidate for this observation (as can be seen in Figure 2). This NIRCcam observation will primarily look for spectral features to test the N₂ dominated atmosphere theory, as CO and CO₂ emission and absorption features can be seen.

Method

Determining the composition of an exoplanet's atmosphere requires obtaining a spectrum of the planet, which can be either an emission or absorption spectrum. In this case, an emission spectrum of the 55 Cancri e will be obtained by performing emission spectroscopy. Emission spectroscopy is a technique that involves analyzing the light emitted by a planet's atmosphere in order to determine its composition.

To perform emission spectroscopy an observation of a secondary eclipse of the planet will be used, which occurs when a planet passes behind its star. By observing this event, we can capture the light from both the dayside of the planet and the star before the planet passes behind the star (out of eclipse). As the planet passes behind the star, only the light from the star can be observed (in eclipse). Finally, as the planet emerges from behind the star, we can capture the light from both again. This process is illustrated in Figure 3, which shows the light curve of a star-planet system during transit and occultation (a secondary eclipse). Taking the difference between the light from out of eclipse and in eclipse will isolate the light that the planet is re-emitting from its atmosphere and allows us to obtain an emission spectrum of the planet. This spectrum can then be used to determine the composition of the atmosphere, including the presence of specific molecules and elements.

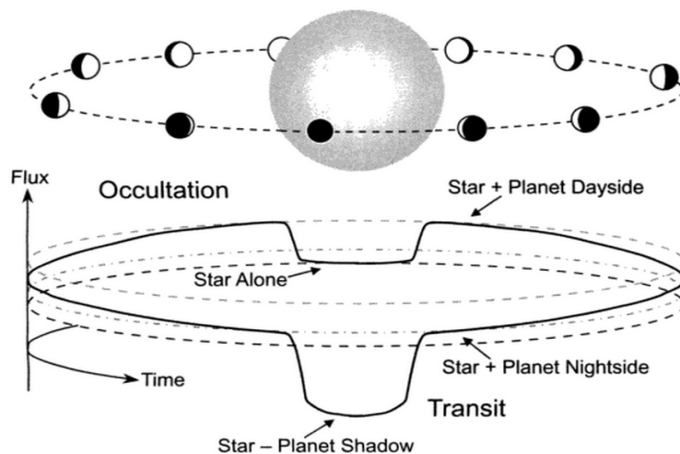


Figure 3: Illustration of a light curve and star, planet system during a transit and secondary eclipse (occultation).

In November of 2022, JWST was used to conduct this observation in the near-infrared wavelength. This observation was carried out using the NIRCcam instrument and the F444W filter. The observation was done in a time series for 5.8 hours during the eclipse event, which provided a baseline before and after the eclipse, enabling accurate measurement of the eclipse depths. The F444W was specifically chosen to observe in the 3.8 to 5.1 wavelength range, allowing for the detection of spectral features of CO and CO₂. JWST NIRCcam employs a grism to spread the light

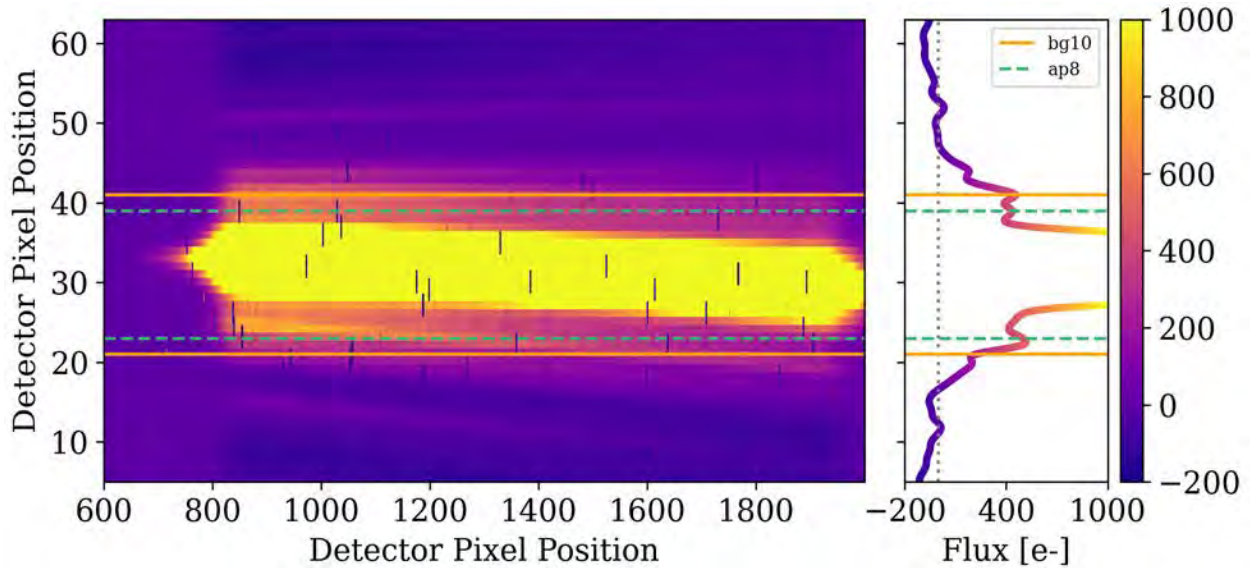


Figure 4: Images received from JWST after calibration. Dashed line shows the extracted region, and the solid line shows where the background region begins. The image is not saturated, but capped at 1000 electrons to show the background

from the observation over the entire wavelength range of our filter. The time series observation gives a detailed account of how much light is emitted in each wavelength by both the star and the planet at each moment of the observation.

After receiving the observation images (as shown in Figure 4), we extract the light from each time series image of the star and planet system. The extracted light is then divided into multiple wavelength bins for each image to determine how much light was received at each time in each wavelength range, also known as a channel. Using this data, we create a spectroscopic light curve (as shown in Figure 5) for each channel, which is a plot of how much light was received in that channel over time. This process is repeated for each channel, and a white light curve is created by summing all the channels, providing a complete picture of the light received over all wavelengths.

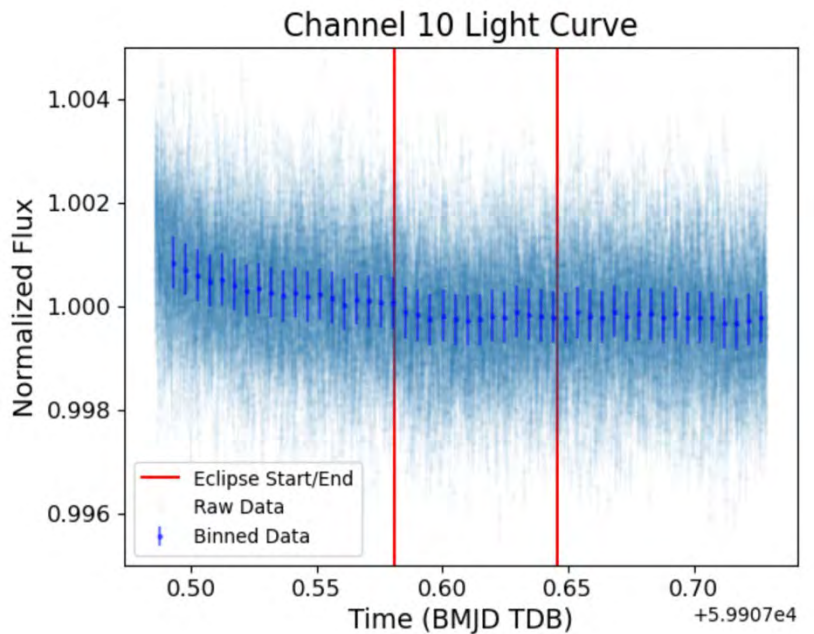


Figure 5: Spectroscopic light curve binned and un-binned for Channel 10 (~ 4.28 microns) with start and end of eclipse shown in Barycentric Modified Julian Date in Barycentric Dynamical Time

After creating the spectroscopic light curves and a white light curve using the extracted light from each image, we fit an eclipse model to each light curve. These eclipse models take into account various planetary parameters and fit each parameter and a linear trend to an eclipse model for each light curve. The fitting process is done using emcee [10] in combination with either batman [11] or PyLightcurve [12]. The resulting fits calculate the eclipse depth for each light curve, which can

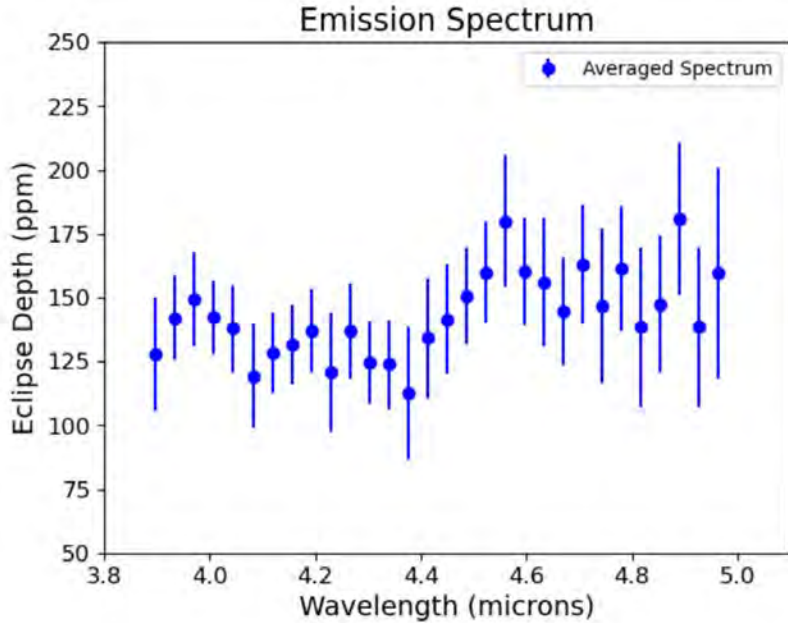


Figure 6: Emission spectrum of 55 Cancri e from the average of four spectra with different noise removal techniques.

then be plotted over wavelength for each spectroscopic channel. The resulting plots provide us with the emission spectrum we need to study the planet’s atmosphere (Figure 6).

Noise is an issue that can affect the quality of any telescope’s observations, even the most advanced ones. Various factors can contribute to noise such instrumental, background, or stellar noise. It is essential to identify the sources of noise in our observations to correct for them. In the case of our observation, we have identified two sources of instrumental noise that we can correct for: $1/f$ noise and housing temperature. These noise sources have been previously observed NIRCcam time series observation.

Schlawin et. al states: “ $1/f$ noise is the largest random error to impact NIRCcam grism time-series measurements” [13]. $1/f$ noise is caused by the detector’s read out system that adds correlated noise to the images. This phenomenon creates noise along the y direction of the image, where each row of the image has a different random value added during the read-out process [13]. Figure 7 shows the images before and after correcting for the $1/f$ noise. To mitigate the noise caused by this phenomenon we can perform “Row-by-row Subtraction”. This is done by determining the median value of all the pixels in a given row that does not contain any light from the system and subtracting the entire row by that median value. This process is repeated for every row in every group for each image, reducing most of the noise along the y-axis of the images.

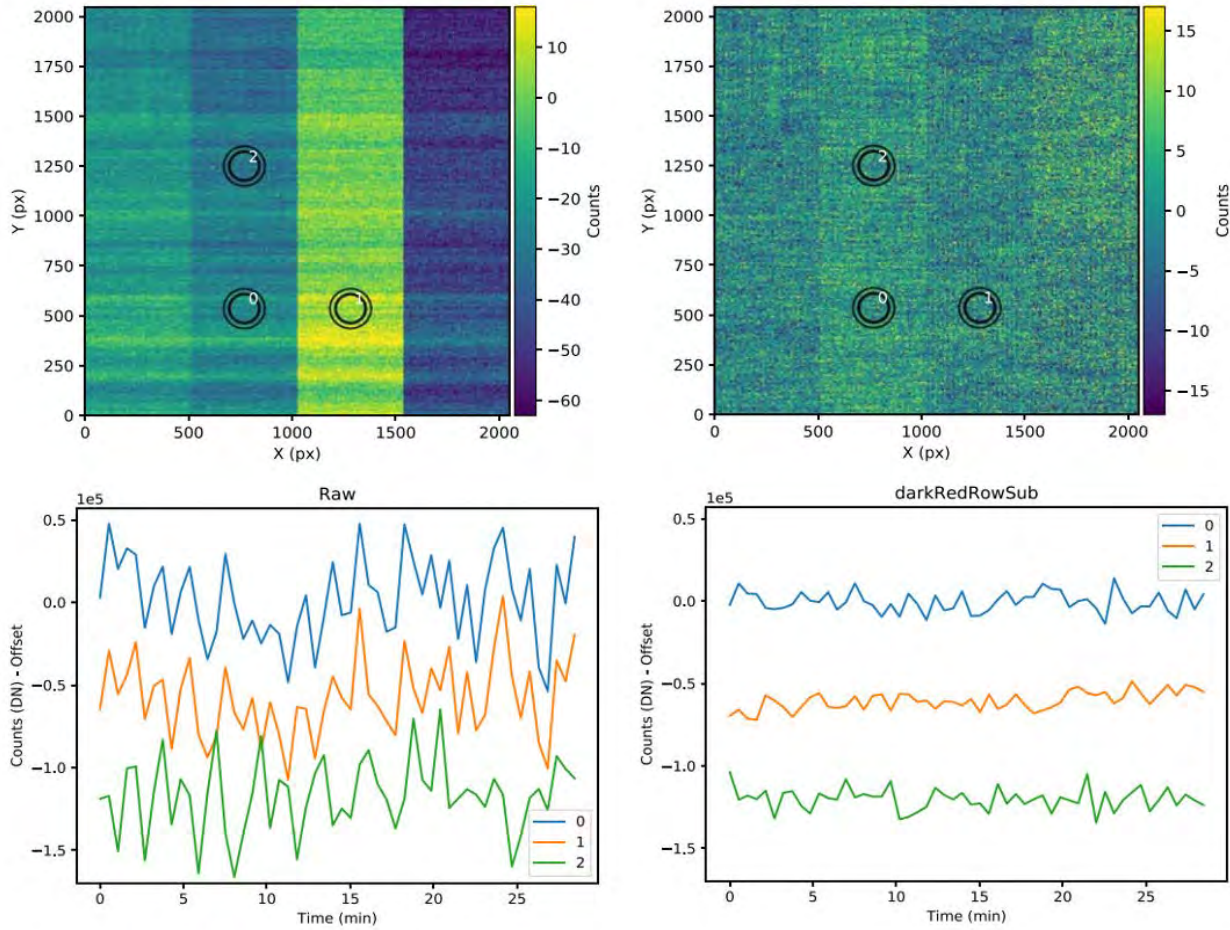


Figure 7: Simulated images of a long dark exposure for JWST NIRCcam time series observations. The left shows the data with no correction and the right shows the image after row-by-row subtraction. [13]

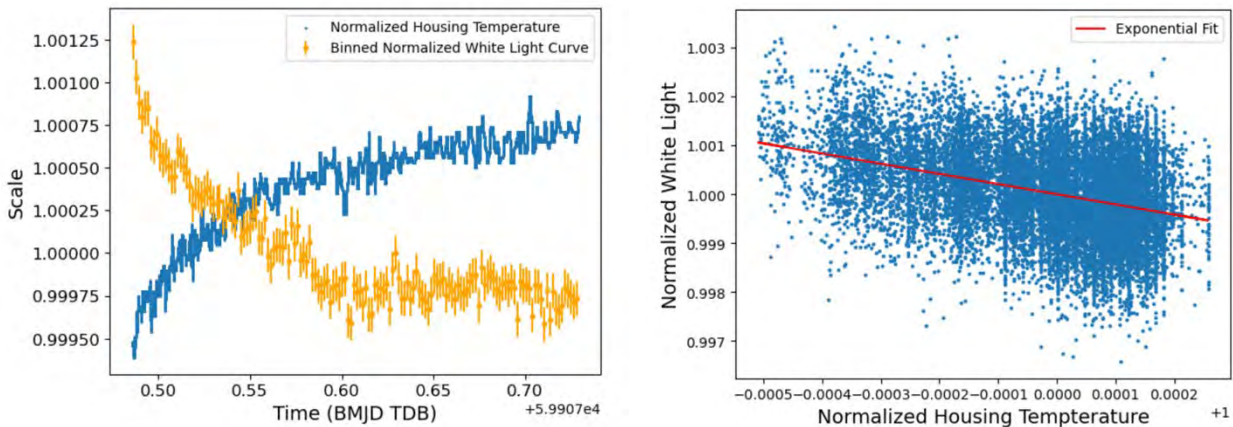


Figure 8: On the left is the normalized NIRCcam housing temperature (blue) scaled by $\times 2$ and the binned white light curve (orange). The two are plotted on the right with an exponential fit in red

The housing temperature has an inverse correlation with the flux of each image over time. As the observation progresses the housing temperature increases slightly by about 0.3 Kelvin over the course of the 5.8-hour observation period. The rate of increase is not linear, with the temperature rising rapidly at first and then slowing down exponentially. This affect is most evident in the light curves, where there seems to be a fast initial downward trend that slows down over time. Figure 8 compares the housing temperature and the binned white light curve over time. Since this affect was not expected before the telescope was launched, there is no established method for correcting this trend. One approach I used was to plot the white light curve flux versus housing temperature and fit several curves to that data, with the best fit being an exponential curve (Figure 8). The white light curve and each spectroscopic light curve were then divided by this fit using the equation: $f(T) = 8 \times T^{-2.079}$. This effectively removed the downward trend in the light curves (Figure 9) and flattened the normalized light curves to 1; however, it also created a larger scatter between the points in the y-direction.

As noise reduction is crucial for analyzing light curves, an additional technique was tried to improve the results. This method is known as “dividing by white”, where every spectroscopic light curve is divided by the white light curve. By dividing every spectroscopic light curve by the white light curve, noise that appears in all wavelengths is removed. However, this method does not eliminate noise that is specific to one wavelength. Although this method cleans up the light curves considerably (Figure 10), one drawback to this method is that the absolute magnitude of the eclipse depth is lost. Instead, our eclipse depths in each spectroscopic light curve are relative to the white light curve. Nevertheless, the shape of the emission spectrum is still visible and is centered around zero. This noise reduction method allows us to identify absorption and emission features within the spectrum with better accuracy.

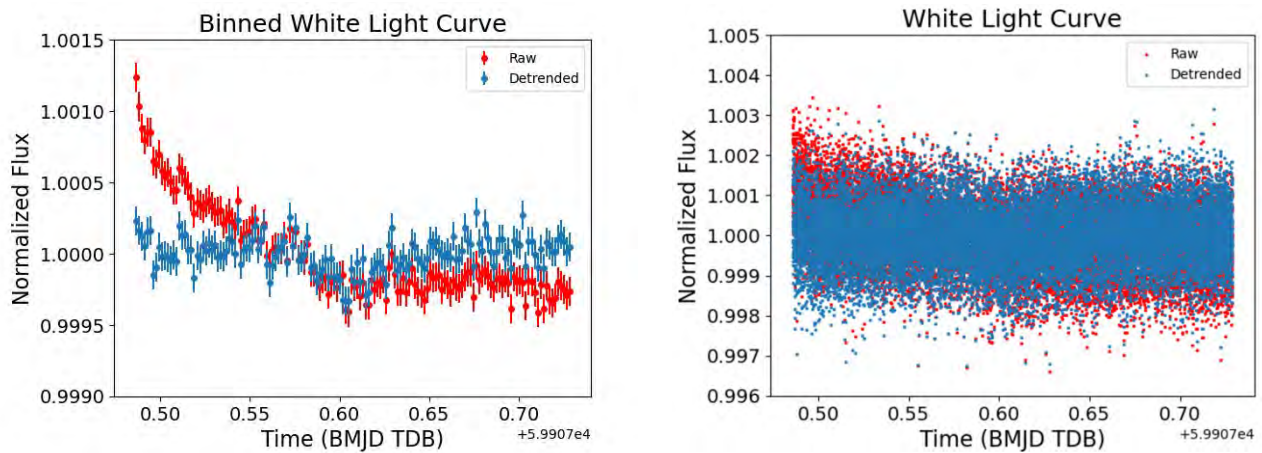


Figure 9: White light curve before (red) and after temperature detrending (blue). Image on the left is binned while the right is un-binned.

Data Reduction

During the observation of the secondary eclipse event with JWST, 20,471 images were received, each pertaining to a specific time during the event. To process these images, two pipelines were used. 1) STSCi's JWST Science Calibration Pipeline [14], 2) Eureka! [15]. Eureka! is an open-source pipeline designed to perform spectral extraction and fitting for JWST exoplanet time-series observations [15]. The processing was divided into 6 different stages. The first two stages could be done using either pipeline, while Stages 3-4 were processed exclusively using Eureka!, and Stages 5-6 were either processed using Eureka! or independently. The six Eureka! stages are outlined as follows:

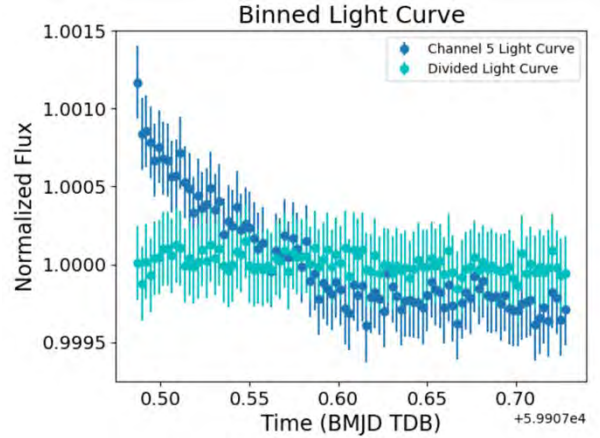


Figure 10: Spectroscopic light curve binned for Channel 5 (~ 4.06 microns) showing before (blue) and after (cyan) dividing by the white light curve

Stage 1. Detector processing: This stage checks for saturation and data quality and converts the ramp integrations into count rate slope images.

Stage 2: Data Calibration: This stage performs flat fielding and extracts 2D and 1D stellar spectra from the images.

Stage 3: Data Reduction. This stage performs background subtraction and spectral extraction from each image.

Stage 4: Generating Light Curves: This stage splits the extracted spectra into wavelength bins and creates a spectroscopic light curve for each bin, and a white light curve for the entire filter.

Stage 5: Light Curve Fitting: In this stage, an eclipse model is fit to each of the spectroscopic light curves and the white light curve and eclipse depth is calculated.

Stage 6: Spectra: This stage creates the planet spectrum using the eclipse depth of each spectroscopic light curve.

In our study, we employed four different combinations of noise reduction and detrending techniques. Specifically, we processed two datasets with row-by-row subtraction and two without. For each of these, one was processed using temperature detrending, and the other processed using the divide-by-white method. We reduced each group almost identically up until specific steps.

During Stages 1 and 2, the Eureka! and the JWST pipeline are largely identical with Eureka! providing greater flexibility in terms of choosing which steps to execute and when, while

the JWST processing was downloaded in full. The JWST pipeline was used when not performing row-by-row subtraction. Eureka! was used for the row-by-row subtracted data to enable us to stop the data reduction at the point where the row-by-row reduction had to be done, which was right before the ramp fitting step. Since Eureka! is essentially a replica of the JWST pipeline for the first two stages, but with more control I used the JWST pipeline for the data without row-by-row subtraction to save computational time. We expect no difference in the results between the processes carried out by Eureka! and the JWST pipeline.

In Stage 3, there is significantly more user control compared to the first two stages. This stage is where the light is extracted from the images that have been run through calibration. Users have control over various parameters such as the region from which to extract light, the aperture size for extraction, and where to start the background region. Our selected parameters for Stage 3 are shown in Figure 4, where we chose a range of 800 pixels to 2000 in the x direction, an aperture of 8 pixels from the center in both the positive and negative y-direction, and a background region starting 10 pixels from the center in both directions. All other options within Stage 3 were kept as default. This allowed us to extract as much light as possible from our observation and provide accurate information for the background subtraction. The output of Stage 3 is a plot (Figure 11) showing the amount of light over time in every wavelength with the x-axis representing wavelength, the y-axis representing time, and the color gradient indicating the amount of flux.

Stage 4 creates the light curves from the extracted light in Stage 3. Users have control over the number of wavelength channels to create for the spectroscopic light curves, as well as some outlier rejection parameters which were kept default for our analysis. We chose to create 30 spectroscopic channels dividing the light from Figure 11 into 30 different wavelength bins across the x-axis. This decision was made to achieve high precision in the final emission spectrum while also keeping the computation time manageable. This stage outputs the spectroscopic light curves and white light curve seen in Figures 5,8,9.

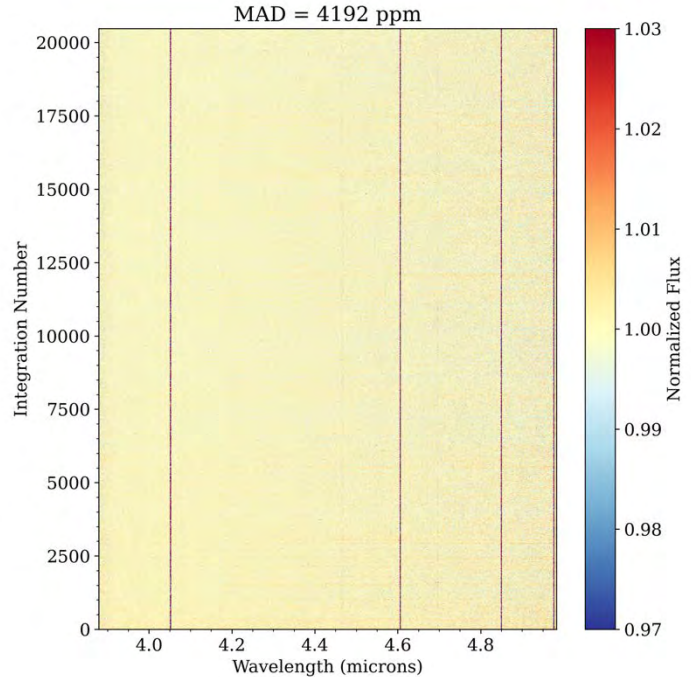


Figure 11: Stage 3 output showing the amount of light (color gradient) versus wavelength (x-axis) and time (y-axis)

Parameter	Symbol	Units	Value
Orbital period	P	days	$0.73654530^{+6.5 \times 10^{-7}}_{-9.5 \times 10^{-7}}$
Transit epoch	$T_0 - 2\,451\,545$	BJD	$4417.0720^{+6.1 \times 10^{-4}}_{-3.6 \times 10^{-4}}$
Planet-to-star radius ratio	R_p/R_s		$0.01874^{+3.9 \times 10^{-4}}_{-2.9 \times 10^{-4}}$
Planetary radius	R_p	R_\oplus	$1.8865^{+0.045}_{-0.035}$
Scaled semimajor axis	a/R_s		$3.4746^{+6.9 \times 10^{-2}}_{-7.2 \times 10^{-2}}$
Semimajor axis	a	AU	$0.01521^{+3.7 \times 10^{-4}}_{-3.4 \times 10^{-4}}$
Orbital inclination	i	deg	$83.56^{+0.61}_{-0.62}$

Table 1: Planetary parameters used for light curve fitting. From Sulis, S., Dragomir, D. et. al 2019 [1]

After Stage 4, we performed our temperature detrending and divide by white noise reduction (Page 9). This greatly improved the dataset and resulted in more reliable results. In Stage 5, we employed various methods to fit the light curves produced in the previous stage. Eureka! contains its own fitting method using emcee and batman to create an emission light curve model based on the given planetary parameters and then fits that model to the given data. Eureka! does not provide a simple solution to importing custom light curves after noise reduction and detrending. Therefore, we used two different techniques to either fit the eclipse with a model or measure the eclipse depth.

The first method was using PyLightcurve to model and fit the light curves using emcee. This method provided equally good and easy to use results as Eureka!’s fitting method. Similar to Eureka!, PyLightcurve created an eclipse model based on the planetary parameters given and fit the eclipse depth as well as a linear fit to the data. Table 1 lists the parameters used for the PyLightcurve modeling, which were given in the paper by Sulis et. al [1]. We used this method for the temperature detrended light curves and provided excellent results. However, for the divide-by-white light curves, a different approach was necessary. This is because when dividing by the white light curve, all eclipse depths become relative to the white light curve. As a result, it is possible to have an eclipse with a negative depth seen in Figure 10.

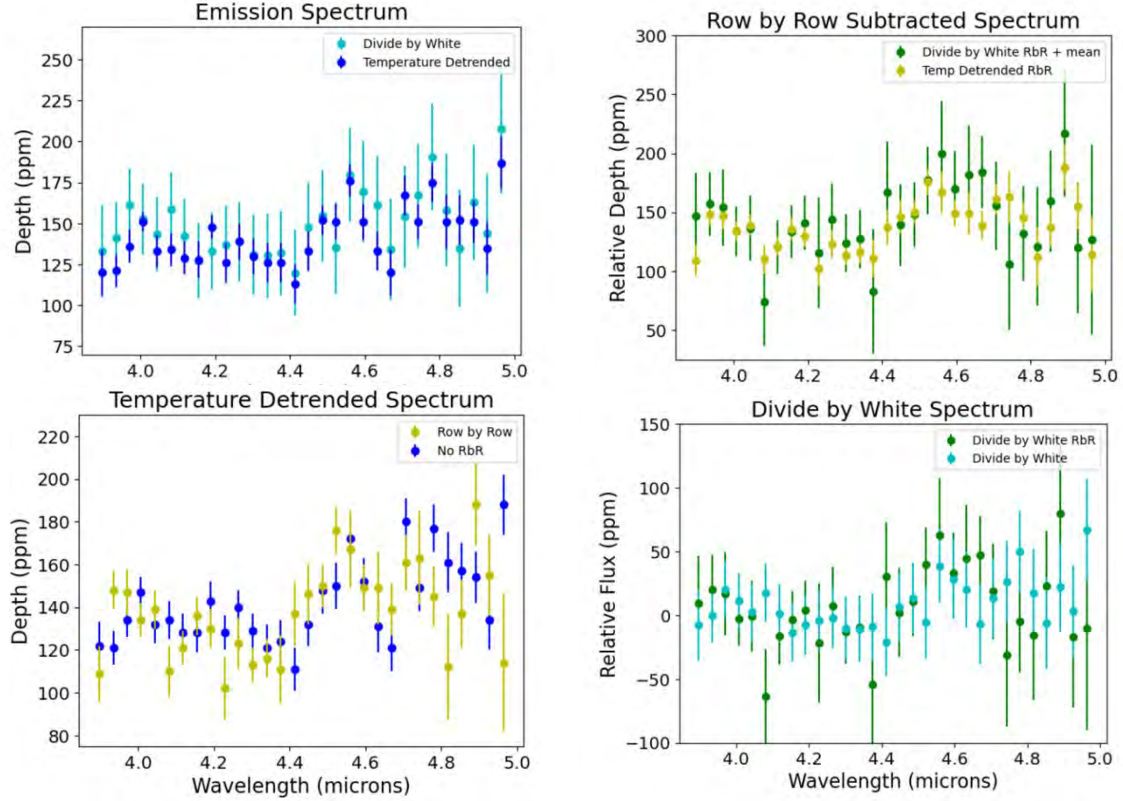


Figure 12: Emission spectra from our four analyses: Top Left (no RbR), Top Right (RbR), Bottom Left (Temperature Detrended), Bottom Right (Divide by White)

Due to the limitation of the PyLightcurve package, we were unable to model inverted eclipses. As an alternative, we divided the data into two separate arrays: one containing only points outside of eclipse and the other only containing points during the eclipse. With those arrays we then subtracted the median of the in-eclipse points from the median of the out-of-eclipse points to obtain the eclipse depth. While this method was effective, it was less precise creating larger error bars in our spectrum, as shown in Figure 12.

Finally, we plotted our transit depths for each spectroscopic light curve using each of the four methods to generate our emission spectra (Figure 12). Additionally, we calculated the mean of all four eclipse depths for each spectroscopic channel and then plotted against wavelength (Figure 13). After producing the spectra, we overlaid the models generated by Hu & Seager (2014), Ito et al. (2015), and Zilinskas et al. (2020b). A model was created for each of the four scenarios: N_2 , N_2 with inversion, O_2 , and SiO . By comparing the models with our spectrum, we can identify the spectral features that provide insight to the composition of the atmosphere, including the elements and molecules present.

Atmospheric inversion occurs when there is an increase in temperature at higher levels of the atmosphere. In Figure 1, a pressure versus temperature diagram of the four models is presented. The two thick atmosphere scenarios without inversion show decrease in temperature as the

atmospheric pressure decreases, corresponding to the height of the atmosphere. On the other hand, the N_2 model with inversion deviates and shows heating after cooling, creating a separate region of the atmosphere that would emit light. Comparing the N_2 models with and without inversion, a large absorption feature of CO and CO_2 is present in the model without inversion. However, for the model with inversion, an emission feature of CO is present coming from the upper atmosphere. This phenomenon is also observed in Earth's atmosphere, where the stratosphere and thermosphere heating up instead of cooling down.

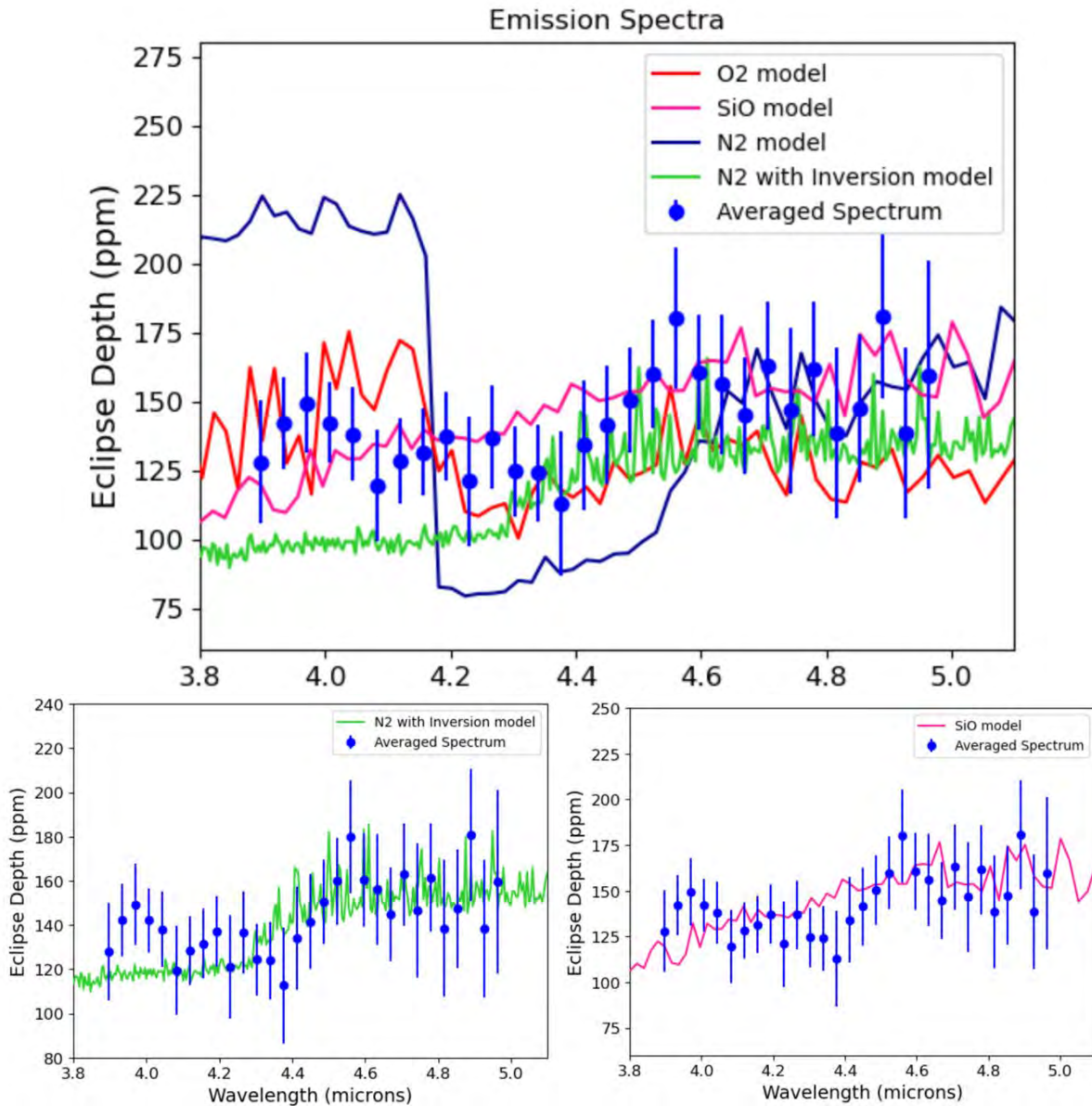


Figure 13: Spectrum acquired by taking the average of the spectrum from the four analyses. Top: All four models overlaid. Bottom Left: N_2 with Inversion fit to spectrum, Bottom Right: SiO model overlaid

Results and Discussion

The emission spectra obtained from our analysis provide results that are consistent with our expectations and are in good agreement with each other. We anticipated eclipse depths ranging from approximately 80-220 ppm depending on the model, and all of our results fall within this range. Transit observations of WASP-39 b with the JWST NIRCcam instrument showed large error bars in their spectrum on the edges of the wavelength range [16]. That same uncertainty can be seen in our data, mostly on the far-right edge. Figure 12 shows our four emission spectra and Figure 13 shows the mean spectrum with the four atmospheric models overlaid.

In the lower wavelengths the N₂ model without inversion displays a rather steady profile around the 200-225 ppm range. Our data ranges from 100 to 175 ppm within the 1 sigma uncertainty in this region, making it unlikely that this model is the best fit. However, the N₂ with inversion model looks promising. The lower wavelengths of our spectra exhibit a rather flat profile with no significant spectral features, which is consistent with the N₂ with inversion model, albeit averaging about 30 ppm higher than our model. From about 4.3 microns, the CO emission feature starts to emerge in the model and our data begins to display much higher peaks and spectral features starting around 4.4 microns. Although this model is not an exact match for our data, it exhibits similar structure to what we observe in our spectra.

The O₂ model appears to show the opposite story of the N₂ with inversion. It has larger spectral features in the lower wavelengths and becomes flatter with smaller peaks and troughs past approximately 4.2 microns. Our data mostly falls within the range of depths in the O₂, but in this case the shape of our spectra does not match the model. In many areas there are peaks in our data where there are dips in the model and vice versa, particularly around 4.1, 4.8, 5.0, and just before 4.3 microns. Therefore, we don't believe that the O₂ model is sufficient to explain our results.

Lastly, we compare our data to the SiO model. This model has a consistent upward trend over these wavelengths without many spectral features starting from about 110 ppm up to 175 ppm. Our spectra also seem to show a similar upward trend over increasing wavelength. This model seems to fit our data well in the lower wavelengths, and fairly well in the higher wavelengths as well. There is however an absorption feature in our spectra centered around 4.35 microns that the SiO model does not cover. Overall, everywhere outside of 4.3 to 4.45 lies within the SiO model within 1 sigma uncertainty, and for that reason, we believe this to be the best fitting model to our data.

Conclusion and Future Work

The study of 55 Cancri e's atmosphere using the JWST NIRCam secondary eclipse observation in the 3.8-to-5.1-micron wavelength range provided significant insight. The aim of the study was to differentiate the thick atmosphere versus the asynchronous rotation scenarios to explain this planet's heat redistribution. Through our analysis of the images taken by JWST, we obtained four emission spectra through the combination of 3 different noise reduction or detrending techniques. These spectra ranged from approximately 100 ppm to near 200 ppm across the different wavelength channels, consistent with expectations.

To determine the atmospheric composition and the cause of 55 Cancri e's heat redistribution, our emission spectra were compared to four atmospheric models created by Hu & Seager (2014), Ito et al. (2015), and Zilinskas et al. (2020b). Our analysis was able to constrain the possible models down to two by eliminating the N₂ model without inversion as well as the O₂ model. The SiO model appears to be the best fit to our data, but the N₂ model with inversion is still promising due to its similarity in structure to our spectra. With each of the two models representing different heat redistribution mechanisms, further observations in different wavelengths will be needed to differentiate the two scenarios.

A new observation of 55 Cancri e using JWST's MIRI instrument's LRS mode was completed in March of 2023. This observation is in the 5-to-12-micron range and will allow us to look at this planet in a new wavelength range with many other indicative spectral features. Figure 2 shows the four models extended to this 5-to-12-micron range. In this range there is a significant SiO emission feature from about 7 to 10 microns, while there are no features for the N₂ with inversion model. This observation enables a clear differentiation between the SiO model and the N₂ with inversion model.

Acknowledgements

I would like to thank Rayburn Reaching Up Fund for supporting my research and the UNM Physics and Astronomy Department as a whole for providing the opportunity to learn and grow through this research. I would like to especially thank Dr. Diana Dragomir for allowing me to work on this amazing project and for her ongoing support and advice.

References

- 1) Sulis, S., Dragomir, D., Lendl, M., Bourrier, V., Demory, B. O., et al. 2019, Multi-season optical modulation phased with the orbit of the super-Earth 55 Cnc e, *A&A*, 631, A129
- 2) Demory, B. O., et al. 2016, A map of the larger day-night temperature gradient of a super-Earth exoplanet, *Nature*, 532, 207-209
- 3) Hu, R., Brandeker, A., Damiana, M., Demory, B. O., Dragomir, D., et al. 2021, Determining the Atmospheric Composition of the Super-Earth 55 Cancri e, *iwst.prop.1952H*
- 4) Nelson, B., et al. 2014, Solved: Mysteries of a Nearby Planetary System's Dynamics, *MNRAS* 441, 442-451
- 5) Angelo, I., Hu, R., 2017, A Case for an Atmosphere on Super-Earth 55 Cancri e, *The Astrophysical Journal*, 154, 232A
- 6) Kite, E. S., Fegley Jr, B., Schaefer, L., & Ford, E. B. 2016, Atmosphere-interior exchange on hot, rocky exoplanets, *The Astrophysical Journal*, 828(2), 80.
- 7) Brandeker, A., 2019, An asynchronous rotation scenario for 55 Cancri e, *ESS*, 51 311-07.
- 8) Ito, Y., Ikoma, M., Kawahara, H., Nagahara, H., Kawashima, Y., & Nakamoto, T., 2015, Theoretical emission spectra of atmospheres of hot rocky super-Earths, *The Astrophysical Journal*, 801(2), 144.
- 9) Hu, R., & Seager, S., 2014, Photochemistry in terrestrial exoplanet atmospheres. III. Photochemistry and thermochemistry in thick atmospheres on super Earths and mini Neptunes, *The Astrophysical Journal*, 784(1), 63.
- 10) Foreman-Mackey, D., Hogg, D. W., Lang, D. & Goodman, J., 2013, emcee: The MCMC Hammer. 125, 306.
- 11) Kreidberg, L., 2015, batman: BASic Transit Model cALculatioN in Python. 127, 1161
- 12) Tsiaras, A. et al. 2016, A New Approach to Analyzing HST Spatial Scans: The Transmission Spectrum of HD 209458 b, *ApJ*, 832, 202T
- 13) Schlawin, E. et al., 2020, JWST Noise Floor. I. Random Error Sources in JWST NIRCcam Time Series, *The Astronomical Journal*, 160:231, 19pp.
- 14) <https://jwst-pipeline.readthedocs.io/>
- 15) Bell, T. J. et al., 2022, Eureka!: An End-to-End Pipeline for JWST Time-Series Observations. arXiv e-prints arXiv:2207.03585
- 16) Ahrer, E., Stevenson, K., et al. 2023, Early Release Science of the exoplanet WASP-39b with JWST NIRCcam, arXiv:2211.10489
- 17) Zilinskas, M., Miguel, Y., Lyu, Y., & Bax, M., 2020b,. Temperature inversions on hot super-Earths: the case of CN in nitrogen-rich atmospheres. arXiv preprint, arXiv:2010.15152.

Other Packages Used

- 1) [ExoTETHyS, Morello et al. 2020](#)
- 2) [Matplotlib, Hunter 2007](#)
- 3) [Numpy, Oliphant 2006](#)
- 4) [SciPy, Virtanen et al. 2020](#)
- 5) [Astropy, Astropy Collaboration 2013](#)
- 6) [ExoClock Project, Kokori et al. 2020](#)